Journal of Manufacturing Processes 18 (2015) 141–150

Contents lists available at ScienceDirect

Journal of Manufacturing Processes

journal homepage: www.elsevier.com/locate/manpro

Technical Paper

Application of local mechanical tensioning and laser processing to refine microstructure and modify residual stress state of a multi-pass 304L austenitic steels welds

Jibrin Sule[a,*], Supriyo Ganguly[a], Harry Coules[b], Thilo Pirling[c]

[a] Welding Engineering and Laser Processing Centre, Cranfield University, Bedford, MK43 0AL, UK
[b] Solid Mechanics Research Group, University of Bristol, Bristol, BS8 1TH, UK
[c] Institut Max von Laue-Paul Langevin, 6 rue Jules Horowitz, BP156, F-38042 Grenoble, France

ARTICLE INFO

Article history:
Received 15 January 2015
Received in revised form 4 March 2015
Accepted 4 March 2015

Keywords:
Austenitic stainless steel
Residual stress
Multi-pass welding
Microstructure
Rolling
Laser processing

ABSTRACT

AISI Type 304L austenitic stainless steels are extensively used in industries, and welding is an indispensable tool used for joining these materials. In a multi-pass weld, the development of residual stress to a large extent depends on the response of the weld metal, heat affected zone and parent material to complex thermo-mechanical cycles during welding. Earlier researchers on this area used either mechanical tensioning or heat treatment to modify the residual stress distribution in and around the weld. In this research, microstructural refinement with modification of residual stress state was attempted by using high pressure cold rolling followed by laser processing in 12 mm thick 304L austenitic stainless steels which is a novel technique. The hardening of the weld metal was evaluated after welding, post weld cold rolling, and post weld cold rolling followed by laser processing. The residual stress was determined non-destructively by using neutron diffraction. Residual stress analysis show that post weld cold rolling was effective in modifying the longitudinal residual stress distribution throughout the entire thickness. Post weld cold rolling followed by laser processing performed in this research was to induce recrystallization of the cold rolled grains. However, post weld cold rolling followed by laser processing showed minor grain refinement but was not effective as it reinstated the stress state.

1. Introduction

Austenitic stainless steel types are the most widely used stainless steels which contain nominally 18% chromium and 8% nickel. These material exhibits an attractive combination of good strength, ductility, toughness, excellent corrosion resistance and good weldability [1,2]. Due to these attributes, austenitic stainless steels are used in a range of industries such as thermal power generation, biomedical and petrochemical, automotive, and chemical engineering [3].

In 300 series austenitic stainless steel grades, AISI 304L stainless steels are extensively used in industries due to their superior low temperature toughness in addition to high corrosion resistance. The carbon content in this alloy is restricted to 0.03%C maximum to avoid chromium carbide formation which leads to lowering of corrosion resistance in localised area. Example of application of these materials include storage and transportation of liquefied natural gas [4] which was reported that, an estimate of more than 20,000 t of 304 and 304L austenitic stainless steels are used per year [5].

Among the various fabrication methods, fusion welding is one of the most widely used joining processes to fabricate stainless steel structures. The welded joints in any installation, is the area of critical importance, since they are likely to contain a higher density of defects than the parent metal and their physical properties can differ significantly from the parent metal. Differences in both welding consumables and the welding process may affect the final weld composition and due to competitive crystal growth which occurs during solidification, preferred crystallographically orientated structures are always observed.

During welding, the rapid solidification caused by the weld thermal cycle induces residual stresses within the weld metal. The magnitude (residual stress) of which must be known if the significance of defects is to be assessed. Such stresses are often reduced or possibly eliminated by a post-weld heat treatment [6] or by other method before the component is put into service. In addition, sensitization of the weldments is one of the potential problems in the welding of austenitic stainless steels. Sensitization leads

* Corresponding author. Tel.: +447741931257.
E-mail addresses: Jibrinsule2005@yahoo.com (J. Sule), s.ganguly@cranfield.ac.uk (S. Ganguly), harry.coules@bristol.ac.uk (H. Coules), pirling@ill.eu (T. Pirling).

http://dx.doi.org/10.1016/j.jmapro.2015.03.003
1526-6125/

Table 1
Chemical composition (wt %) of AISI 304L grade of austenitic stainless steel plate.

C	Si	Mn	Cr	P	Mo	Ni	Al	S	Cu	Nb	Ti
0.021	0.36	1.48	18.2	0.022	0.15	8.10	< 0.01	<0.005	0.19	0.01	<0.01

to degradation of corrosion resistance as well as the mechanical properties of the welded samples [7,8]. Although depending upon the application; titanium, niobium or tantalum can be added to resist sensitisation which results into loss of corrosion resistance properties in localised area [2]. The sensitised microstructure along with presence of residual stress will hasten crack propagation. For example, austenitic stainless steels with residual stresses under a corrosive service environment may fail by stress corrosion cracking (SCC). This type of failure occurs under the combined action of corrosion and externally applied stresses in susceptible materials.

Therefore, the knowledge and the method to eliminate the residual stresses field in a welded joint is important in avoiding distortion, and to prevent premature failure due to in-service degradation mechanisms such as fatigue, stress corrosion cracking.

A number of methods have been used to mitigate the effects of residual stress in stainless steels. These include; low temperature stress relief with slow cooling, and solution annealing [9]. The use of filler metals was also developed to reduce the residual stresses generated during welding [10]. Vibratory stress relief (VSR) which is a process to reduce and redistribute the internal residual stresses of welded stainless steel structures by means of post-weld mechanical vibration was reported [11,12]. The water-shower cooling during welding was also reported to reduce tensile residual stress in austenitic stainless steel welding [13]. However, application of local mechanical tension (rolling) on multi-pass welds of stainless steel is a novel approach.

Post weld cold rolling followed by laser processing presented in this paper was carried out to induce recrystallization of the cold rolled grains. Generation of such microstructure would increase the strength and toughness of the material which is lower in as-welded state due to the formation of dendritic grain structure in multi-pass welds.

The aim of this research is the modification of residual stress (creation of compressive residual stress in and around the weld) and creation of a re-crystallised microstructure by applying a novel technique of local mechanical tensioning (post weld rolling method) followed by laser processing to modify the stress field and refine the microstructural constituents in a multi-pass of 304L austenitic stainless steel.

2. Experimental procedures

2.1. Material

The material used for this research was AISI 304L grade of austenitic stainless steel plate (12 mm thick) and the filler wire used was Lincoln MIG 308L Si of 1.0 mm nominal diameter. Table 1 shows the chemical compositions of the AISI 304L grade. Table 2 shows the chemical compositions of the filler wire. The shielding gas used was 98% Ar and 2% O_2 at flow rate of 30 l min^{-1}. The dimension of the test piece used for welding was (300 × 150 × 12) mm^3 which was machined out from the 304L grade of austenitic stainless steel plate. The setup is shown in Fig. 1.

Table 2
Chemical composition (wt %) of the filler wire.

C	Si	Mn	Cr	P	Mo	Ni
0.01	0.75	1.6	20	0.015	0.20	10

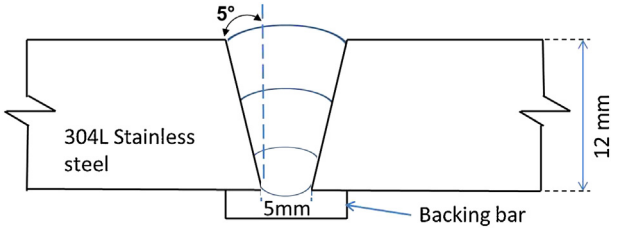

Fig. 1. 304L grade of austenitic steel plate set-up with backing bar.

2.2. Experimental method

2.2.1. Welding

The welding process used was the Tandem Gas Metal Arc Welding (GMAW) DC electrode positive. An optimised GMAW torch as shown in Fig. 2 was used for welding. The contact tips were fed by two independent power sources and two independent wire feeding units. During welding the lead arc determines the depth of penetration while the trail arc controls the final weld bead shape [14]. Significant research on this welding process has been reported and can be found in [15,16]. The welding parameters used are shown in Table 3

The heat input was also calculated using Eq. (1).

$$\text{Heat input} = (\text{current} \times \text{voltage} \times \text{efficiency})/(\text{Travel speed}) \quad (1)$$

The efficiency used in this research was 80% of the total heat input according to Kou [8].

2.2.2. Rolling (local mechanical tensioning)

The rolling machine used was capable of rolling with a constant load. The principle of operation of this machine is that, the hydraulic cylinder applies a vertical force through a single roller supported in a fork assembly. The roller was made from hardened BS 4659 BH13 tool steel. It has an effective width of 30 mm and its diameter is 100 mm. The welded plate was firmly clamped on the base plate of the rolling rig as shown in Fig. 3 while the crossbeam with the roller, is translated by a linear drive system.

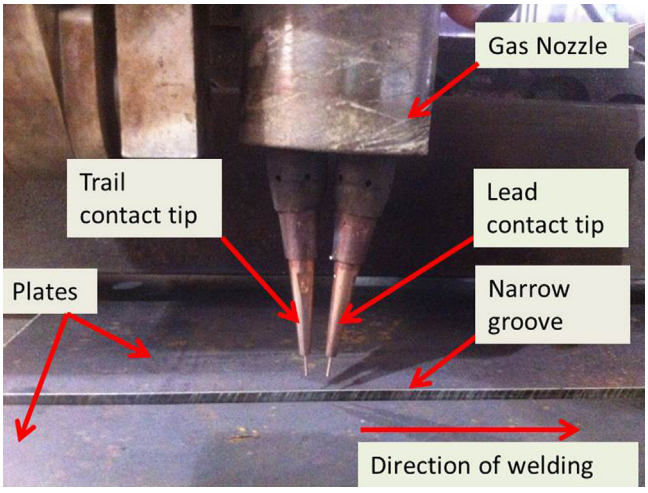

Fig. 2. Typical tandem GMAW torch.

Table 3
Welding parameters on narrow groove welds.

		Lead			Trail			Lead	Trail
Pass	Travel speed ($m\,min^{-1}$)	Wire feed speed ($m\,min^{-1}$)	Average. current (A)	Average. volts (v)	Wfs ($m\,min^{-1}$)	Average. current (A)	Average. volts (v)	Heat input ($kJ\,mm^{-1}$)	Heat input ($kJ\,mm^{-1}$)
Root pass	0.9	11	218.9	21.1	11	216.1	21.0	0.26	0.25
Fill 1	0.9	12	232.3	21.9	12	230.3	22.3	0.28	0.28
Cap pass	0.7	10	222.5	23.5	10	219.8	23.9	0.37	0.37

Post weld cold rolling was carried out on the capping pass of the multi-pass weld using a rolling load of 100 kN with constant travel speed of 0.7 m min^{-1}. A flat roller was used and the rolling force was applied on the top of the weld metal. The roller did not touch the plate surface on either side of the weld. Hence the rolling load was transferred through the capping pass.

2.2.3. Laser processing

An IPG YLR-8000 fibre laser was used for laser processing. The laser beam was delivered to the laser head through an optical fibre of 300 μm diameter. The Laser beam was collimated by a lens of 125 mm focal length and then focused using a 250 mm focussing lens. This produced a spot size of 0.61 mm at the focal spot. However, the laser beam in this specific experiment was used to increase the temperature at a very controlled rate and a defocussed beam of 20 mm spot size was used to reduce the power density at the spot. The vertical distance for defocussing was determined using a beam diagnostic system. The laser set-up is shown in Fig. 4. The laser head was tilted at 10° angle to avoid any back reflection which could damage the lens.

The purpose of laser processing is to induce recrystallization after cold rolling of the weld metal. Localised cold rolling of the weld metal resulted in local plastic deformation which did not only introduces strain energy but also relaxes the tensile residual stress state that formed from the thermal energy applied during welding. Application of laser on the other hand was to induce recrystallization; however, excessive application would result in reinstating the residual stress state which was removed during cold rolling. Therefore, application of laser needed to be precise to achieve a controlled rise in temperature.

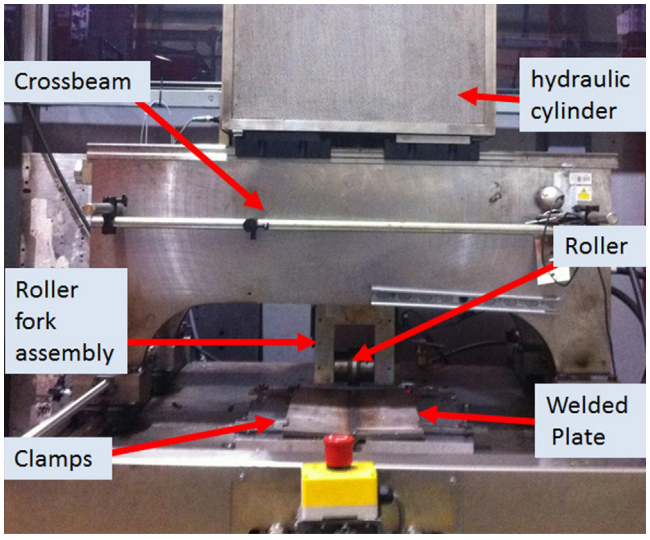

Fig. 3. Overview of the rolling rig set-up showing roller and welded plate.

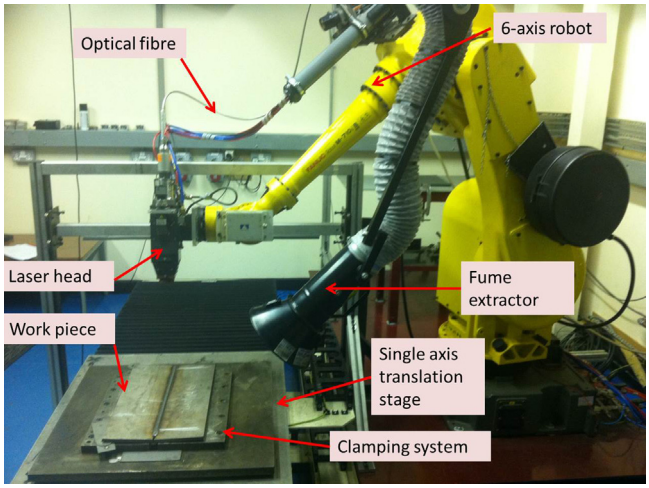

Fig. 4. Laser processing set-up for the experiment.

2.3. Experimental measurement

2.3.1. Weld thermal cycles determination

Thermocouples were used to measure the transient thermal cycle of the weld metal with the aid of a Scopecorder 750 instrument. A hole was drilled through the plate thickness from the root side through the backing bar as shown in Fig. 5, into which K-type thermocouples was placed. The thermocouple was placed at 0.5 mm below the top of the capping pass. Laser travel speed of 0.3 m min^{-1} and 0.4 m min^{-1} were used with laser powers of 1.0 kW and 0.5 kW respectively.

2.3.2. Microstructure and hardness test

The welded samples were cut, ground and polished according to standard metallographic procedures for microstructural observations and micro hardness tests. For micro hardness testing, 500 g load and 5 s dwell time was applied. Across and along the multi-pass weld metal, the hardness scanning was done with an interval of 0.5 mm between consecutive points.

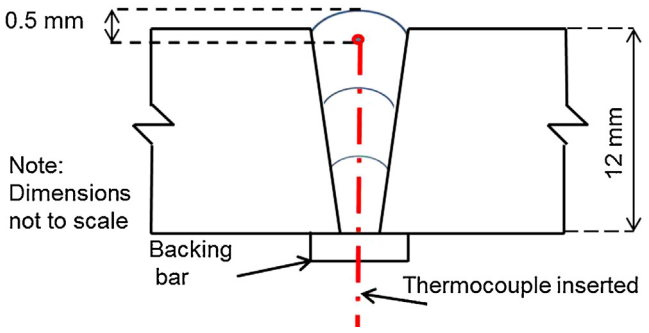

Fig. 5. Sketch showing thermocouple positions in weld metal cross-section.

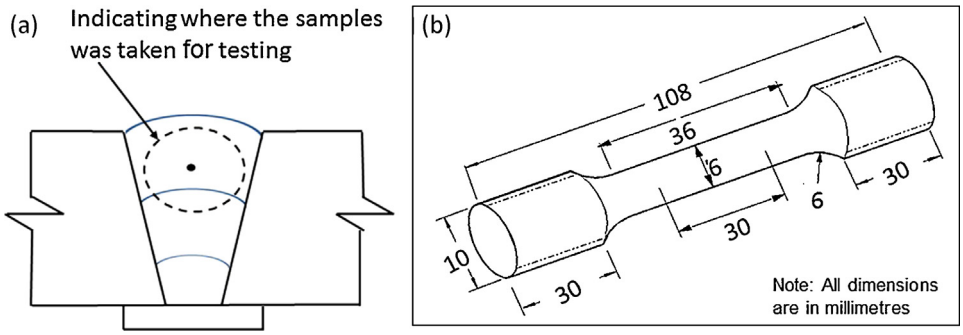

Fig. 6. Tensile test (a) All weld metal in longitudinal direction (b) dimension of tested samples.

2.3.3. Tensile tests

The all weld metal tensile testing samples were machined from the welded plates in accordance to ASTM E8/E8M–08 standards. The tensile tests were designed to ensure that, the samples to be tested are taken as close as possible near the cap pass in longitudinal direction (welding direction of the plate) as shown in Fig. 6(a). As shown in the sketch (Fig. 6(a)), 2/3 of the cap pass and 1/3 of fill 1 form the tested samples.

2.3.4. Measurement of residual stresses

Strain Analyser for Large and Small scale engineering Applications (SALSA) neutron diffractometer at the Institut Laue Langevin in France was used to measure the residual elastic strain [17]. The residual stress state was analysed from the measured elastic strain [18]. Measurements were made on the mid cross-sectional plane of a 200 mm sample (plane PQRS) shown in Fig. 7. This was based on the assumption that, the stress state in the middle will be from steady state welding process. The measurements were taken at 2, 6 and 10 mm below the plate surface on which the capping pass was laid. Longitudinal, transverse and normal strains were measured assuming these directions, by symmetry, to be the principal stress directions. The coordinate axes shown in Fig. 7: L represents the longitudinal direction, T represents transverse direction, and N represents normal direction.

The inter-planar spacing (d) of the {3 1 1} family of crystallographic planes was chosen for measurements of all the principal strain directions since this plane gives the macroscopic average strain over the measured gauge volume [17]. The measurements were made using a neutron incident beam of wavelength, 1.62 Å, which gives a diffraction angle (2θ) of 95.99°. Through-thickness scan was used for accurate positioning of the gauge volume within the plate. The gauge volume dimension was determined by using slits in front of the in-coming beam and collimates the diffracted beam to maintain the through thickness resolution. For this experiment, an incoming beam of $2 \times 2\,mm^2$ was used for the longitudinal strain measurement while a 2 mm collimator was used for the diffracted beam to achieve the desired spatial resolution. For transverse and normal strain measurement an incoming beam of $2 \times 20\,mm^2$ was used, with the assumption that the stress state and magnitude will remain constant in the welding direction. The increase in gauge volume along the welding direction, in these two directions, allows faster measurement with more grain sampling.

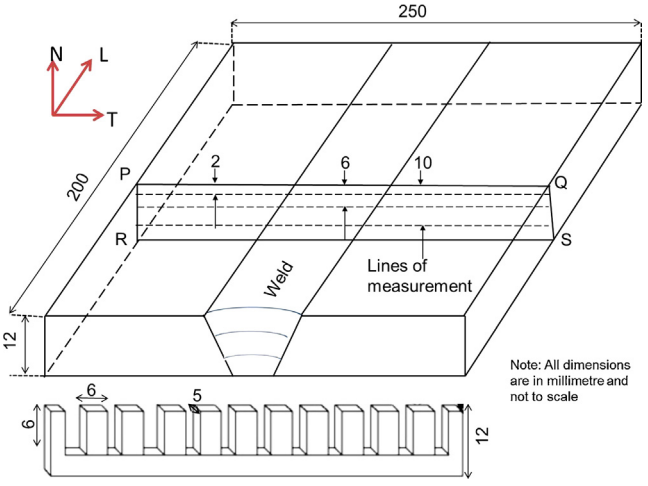

Fig. 7. Schematic diagram of the multi-pass welded plate and the reference comb sample.

The stress-free inter-planar spacing was measured using a comb sample of dimension 6 mm × 6 mm × 5 mm machined out from the parent plate by electrical discharge machining (EDM). The dimension of the individual comb would ensure relaxation of any macro residual stress field and will allow positional correction of the measured strain for compositional variation across the weld and also any changes in lattice parameter due to intergranular straining [19,20]. The stress-free lattice spacing (d_0) was measured in all the three principal strain directions.

The lattice spacing d is related to scattering angle ϕ_{hkl} by Bragg's law [21] as shown in Eq. (2).

$$\lambda = 2d_{hkl} \sin\left(\frac{\phi_{hkl}}{2}\right) \tag{2}$$

Where, λ, is the wavelength of the incident neutron beam; (d_{hkl}) is the inter-planar spacing and ϕ_{hkl} is the angle between incident and diffracted beams.

Gaussian fitting routine was used to fit the intensity profile and precise determination of the peak position. The stress-free lattice spacing (d_0) measurement combined with the lattice spacing measurements were used to calculate strain (ε) for every position across the weld using Eq. (3).

$$\varepsilon_{hkl} = \left(\frac{d_{hkl} - d_{0hkl}}{d_{0hkl}}\right) \tag{3}$$

Where ε is strain, *hkl* are the coordinate planes, *d* is the lattice spacing and d_0 is strain-free spacing (measured in the same plane).

Once the strain is determined, the principal stress was analysed using the Hooke's law for three dimensional state of stress as shown in Eq. (4), using the appropriate elastic constants for the specific crystallographic plane.

$$\sigma_{ii} = \frac{E}{(1+\upsilon)}\left[\varepsilon_{ii} + \frac{\upsilon}{(1-2\upsilon)}(\varepsilon_{11} + \varepsilon_{22} + \varepsilon_{33})\right] \tag{4}$$

Where E and υ are the Young's modulus and Poisson ratio respectively, and $i = 1, 2, 3$ indicate the component of stress and strain relative to chosen to the principal strain directions. Elastic constants values of $E = 200$ GPa and $\upsilon = 0.29$ [22] are used to calculate stress from measured strains.

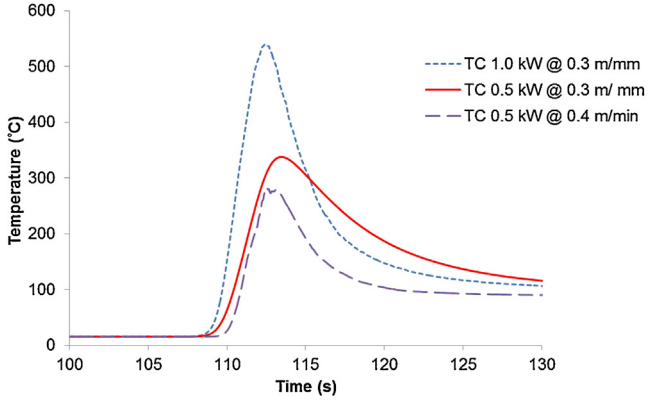

Fig. 8. Thermal cycles of laser powers of 1.0 kW and 0.5 kW with travel speed of 0.3 m min^{-1} and 0.4 m min^{-1} at 0.5 mm below the capping pass.

2.3.5. *Full width at half maximum*

Full width at half maximum of a diffraction peak indicates the plastic strain history of the point in a metallic material [23,24]. Analysis of full width at half maximum reveals information with respect to the inter-granular straining of the alloy [25].

3. Results and discussions

3.1. *Time–temperature plot*

Fig. 8 shows the weld thermal cycle for the two different laser powers and two different laser travel speeds at constant beam diameter of 20 mm. As shown in the figure, the peak temperature of the 1.0 kW at 0.5 mm below the weld surface using a travel speed of 0.3 m min^{-1} was approximately 537 °C (810 K). With the same travel speed and location but using laser power of 0.5 kW, the corresponding temperature reading was 330 °C (603 K). Similarly, with laser power of 0.5 kW at travel speed of 0.4 m min^{-1}, correspond to temperature reading of 295 °C (568 K). In this research, the laser power of 1.0 kW with the travel speed of 0.3 m min^{-1} was chosen for the experimental work described here. This combination was chosen based on the metallographic results.

3.2. *Microstructure observation*

Fig. 9 shows the optical microstructures of the capping pass of the three samples consist of austenite and ferrite structures. These structures are as a result of both the solidification behaviour and subsequent solid-state transformations which are controlled by both composition and weld cooling rates. Under normal condition, austenitic stainless steels will exhibit a single phase that is maintained over a wide temperature range. However, austenitic microstructure containing a small amount of ferrite is less crack sensitive compared to a fully austenitic microstructure. Fig. 9(a), shows a columnar dendritic structure. This is attributed to the fact that, during weld metal solidification, grains tends to grow in the direction perpendicular to pool boundary. This dendritic solidification of the weld metal often leads to segregation of alloying elements within the grain structures which would result in formation of localised region with reduced corrosion protection. Post weld cold rolling shown in Fig. 9(b) has modified the grain structure. It was observed that the deformation cause by cold rolling does not initiate any measurable transformation. Post weld cold rolling follower by laser processing resulted in refining the grains as shown in Fig. 9(c). This refine grains would increase the strength and toughness of the material which is lower in as-welded state due to the formation of dendritic grain structure.

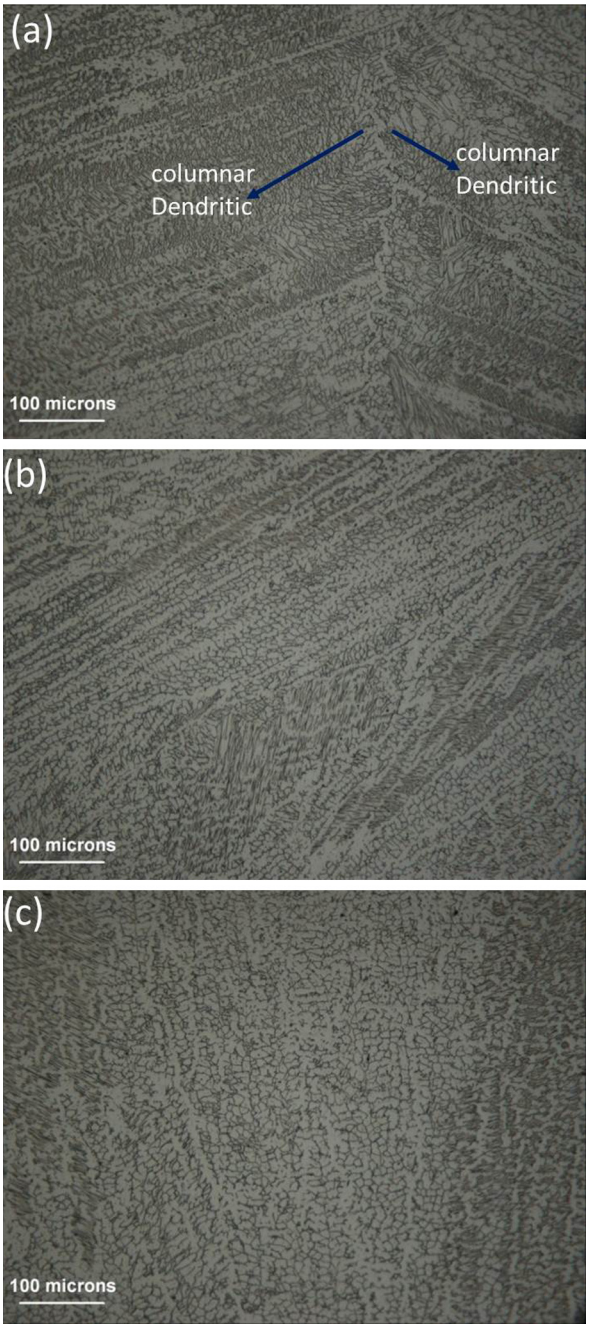

Fig. 9. Optical micrograph of 304L austenitic steel at the cap pass (a) As-welded (b) Post weld cold rolled (c) Post weld cold rolled followed by laser.

For further analysis of grain structure, the crystallographic textures of weld metals were obtained by electron back-scatter diffraction (EBSD). The pole Fig. plots are shown in Fig. 10. The texture intensity of the samples decreases as the sample was rolled and further decrease when post weld rolled followed by laser treatment was applied. This shows that the texture of the austenitic phase can be affected by grain reorientation induced by plastic deformation.

These textures were obtained from data collected over an area of 316 μm × 234 μm with step size 0.73 μm. It is important to emphasize that the grid step size limits the size of the structure elements that can be analysed using EBSD. However, based on the step size used, the average grain size of the as-welded sample was 14.81 μm at cap pass. When the rolling load was applied on the same position, the average grain size was found to be 19.78 μm, similarly; average

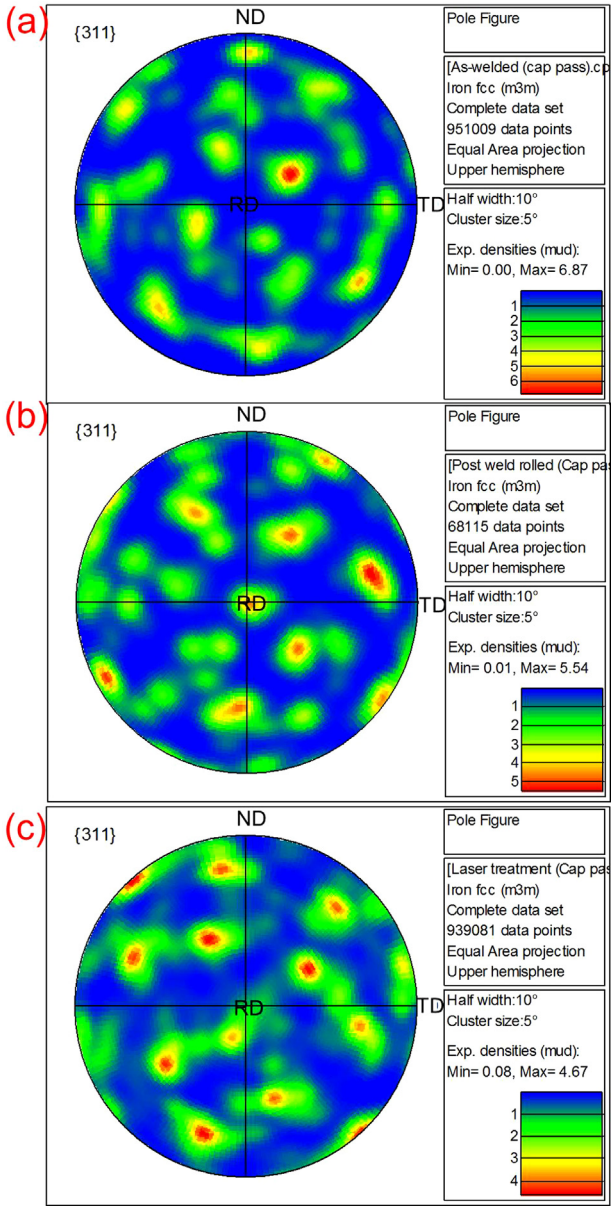

Fig. 10. Pole Fig.s of crystallographic planes obtained by electronic back-scatter diffraction pattern measurement at the cap pass (a) As-welded (b) Post weld cold rolled (c) Post weld cold rolled followed by laser.

grain size of 11.00 μm was found when post weld cold rolling followed by laser processing was applied on the sample at the same position. Among many other factors, grain boundary area poses as one of the major obstacles for movement of dislocations. Although, there is no significant changes in the grain sizes, the reduced grain size (11.00 μm), in laser processed samples would, therefore, has the potential of improving the strength and toughness of the weld metal. It was also evident that, in as welded sample, the grain size increase from root pass to cap pas. The root pass, fill 1 and the cap pass have the grain sizes of 4.20 μm, 10.37 μm and 14.81 μm respectively. This could be attributed to the fact that, thermal cycles from subsequent passes refine the grains from the previous pass.

3.3. Residual stress

The residual stress analysed from the measurements of elastic strain shows a variation in residual stress across the weld at 2 mm below the weld surface (Fig. 11). These are familiar distributions of longitudinal residual stress (σ_{xx}) during welding: showing tensile stresses close to the weld line and slightly compressive further away from it.

The residual stress analysed also showed a reduction in magnitude from cap to root in the as-welded state. As expected, when a cold rolling was applied the localised plastic deformation was evident throughout the entire thickness. However, the effect was more significant at the cap pass causing the tensile residual stress state near the cap to change to compressive stress state (Fig. 12). At the root pass, the tensile residual stress reduces from 208 MPa to 74 MPa as shown in Fig. 12. Generation of compressive stress state at the cap pass is beneficial in improving the structural integrity of a component as most of the in-service deterioration starts with a surface flaw.

As also shown in Fig. 12, the peak tensile residual stress of the as-welded sample diminishes in magnitude through the thickness of a multi-pass weld. This is attributed to the fact that, multiple passes result in thermal straining of previously laid pass from successive passes. The thermal cycling would cause macroscopic plastic deformation of previously laid passes. In other words, subsequent passes have an annealing effect on the previous one, thereby relieving residual stresses from the previous passes.

3.3.1. Effect of post weld cold rolling through the thickness

A flat roller of 30 mm width was used which determines the extent to which localized plastic strain is induced and thereby, generation of compressive longitudinal stress (Fig. 11). However, the compressive zone width is narrower than the width of roller because the contact area of the roller is smaller compared to the width of roller. Hence rolling causes plastic deformation around that region of the weld which is approximately 20 mm in width.

As shown in Fig. 11, post weld cold rolling has changed the longitudinal residual stress state causing it to become compressive around the weld metal (from peak tensile stress of 395 MPa to compressive stress of 80 MPa). Application of rolling to the welded joints causes weld metal to yield thereby relieving the residual stress state that exists in the region. In other word, these rolling processes, compresses the material in the direction normal to the weld's surface, thereby causing it to expand in the plane of the weld, relaxing any tensile residual stresses in the plane.

It was evident that, at about 6 mm below the weld surface (Fig. 12), the rolling load has significant influence on the residual stress state of the weld (changing the peak tensile stress from 319 MPa to 50 MPa). These suggest that, the closely packed atom of the material (304L austenitic) make it easier to deform through the thickness which enables the reduction in the residual stress to extend through the thickness. Deformability of austenitic steel is higher than the ferritic steel because of more active slip planes in austenitic steel.

Similarly, at 10 mm below the weld surface; the rolling load changes the residual stress state (peak tensile stress from 208 MPa to 74 MPa) suggesting little impact of the rolling in this region. It can therefore be deduced from this work that post weld cold rolling was effective in modifying the residual stress.

3.3.2. Effect of post weld cold rolling followed by laser processing

Laser processing after cold rolling has been shown to increase the longitudinal residual stress from compressive stress of 80 MPa to peak tensile stress of 479 MPa (Fig. 11) indicates a high thermal input and non-uniform cooling of the material, thus generating inhomogeneous plastic deformation and tensile residual stresses.

With reduced heat input below the weld surface (6 mm), change on the longitudinal residual stress state was observed, modifying the peak tensile stress from 50 MPa to 220 MPa (Fig. 12). This could be attributed to low thermal conductivity and high coefficient of thermal expansion of the austenitic steel.

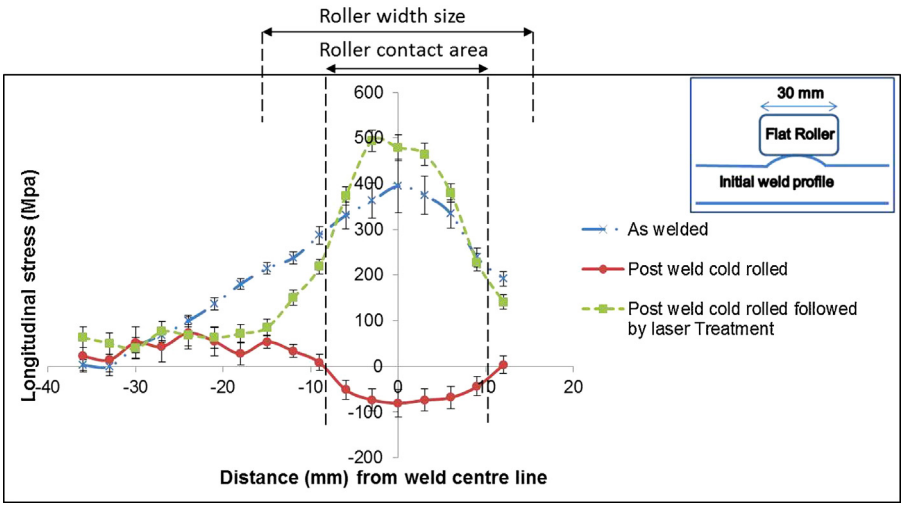

Fig. 11. Residual stress profile across the weld in sample with different processing conditions (measured 2 mm below the top surface).

Similarly, at about 10 mm below the weld surface (Fig. 12), application of laser processing to the cold rolled samples reinstated residual stress distribution profile to as-welded state. Indicating that, the heat conducted through the material at that region was not sufficient to cause any changes in the residual stress state.

3.4. Full width at half maximum (FWHM)

FWHM values of the diffraction peaks were obtained from Large Array Manipulation Program (LAMP) software. Fig. 13 shows the effect of FWHM on (a) as-welded sample at different depth (b) Post weld cold rolling at different depth and (c) the three samples at 2 mm below weld surface.

As shown in as-welded sample in Fig. 13(a), the FWHM at 10 mm below the weld surface was higher than the FWHM at 2 mm below the weld surface. Since the root regions experience more thermal cycles than any other region, the root pass undergo more thermal straining compare to cap pass. Fig. 13(b) shows a significant increase in FWHM profile at the cap pass when the cold rolled was applied to the weld metal. This shows that, the FWHM increases with hardening (increasing plastic deformation). Of course, because of the direct contact between the cap pass and the roller, the cap pass of the weld experience more deformation as compared to passes below the cap pass. In addition, as the effect of the applied load by the roller diminishes through the thickness

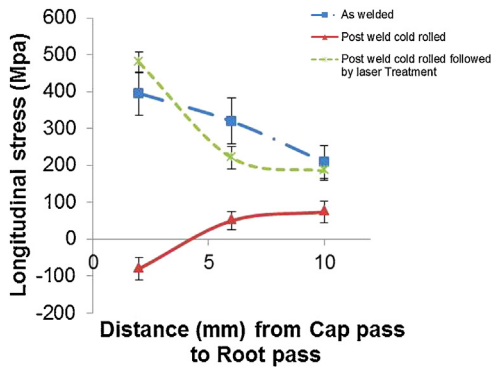

Fig. 12. Variation of peak residual stress magnitude through the thickness (measured at 2, 6, and 10 mm below the top surface).

as shown in Fig. 13(b), the peak FWHM decreases; indicating that FWMH is influenced by the work hardening effect of the cold rolling process. Therefore, the dominant factor affecting FWHM of plastically deformed sample is lattice relaxation induced by misfit dislocation. However, FWHM profiles are not only influenced by plastic deformation but it is also sensitive to residual stress [26]. In this experiment, an increase in FWHM as shown Fig. 13(b), modified the tensile residual stress to compressive residual stress (cap pass) as it is evident in Fig. 11. Furthermore, as FWHM profile reduces when cold rolling followed by laser processing was applied in Fig. 13(c), the tensile residual stresses increase (Fig. 11). This could be due to the high thermal input from laser.

3.5. Hardness

A hardness scan was performed from the cap pass to the root pass as shown in Fig. 14. The effect of cold working was observed throughout the entire thickness of the material when load of 100 kN was applied. This may be attributed to closely packed plane of the material since it is easier for dislocation to move. However, the cold working was most significant at the cap pass because of direct roller contact with cap pass when compared with other passes.

Application of laser after cold weld rolling shows decrease in hardness values (300HV to 280HV) at the cap pass. This diminished in hardness values, could be attributed to change in microstructure. Although, the thermal energy applied was not sufficient to supply enough energy to sustain a complete recrystallization kinetic as it was evident in the change in grain sizes measured.

Fig. 15 shows the hardness distribution at the cap pass. Fig. 15(a) shows the hardness scan line (measurement at 1 mm below the plate surface) on the sample while Fig. 15(b) shows the hardness profile. The heat-affected zones (HAZ) in all the three samples were harder than the base metal. This could be attributed to the strain-hardening of the HAZ.

Hardness in the weld metal can also be attributed to the formation of strain-induced martensite as result of cold deformation. Although a number of researches have been carry out on the formation of martensite in stainless steels upon cold work [27–29], but it was not clear in literature about the amount of plastic deformation that could introduce martensite in stainless. However, in this research, it can be deduce that the quantity of martensite formed largely depends on the temperature and on the nature and rate of deformation.

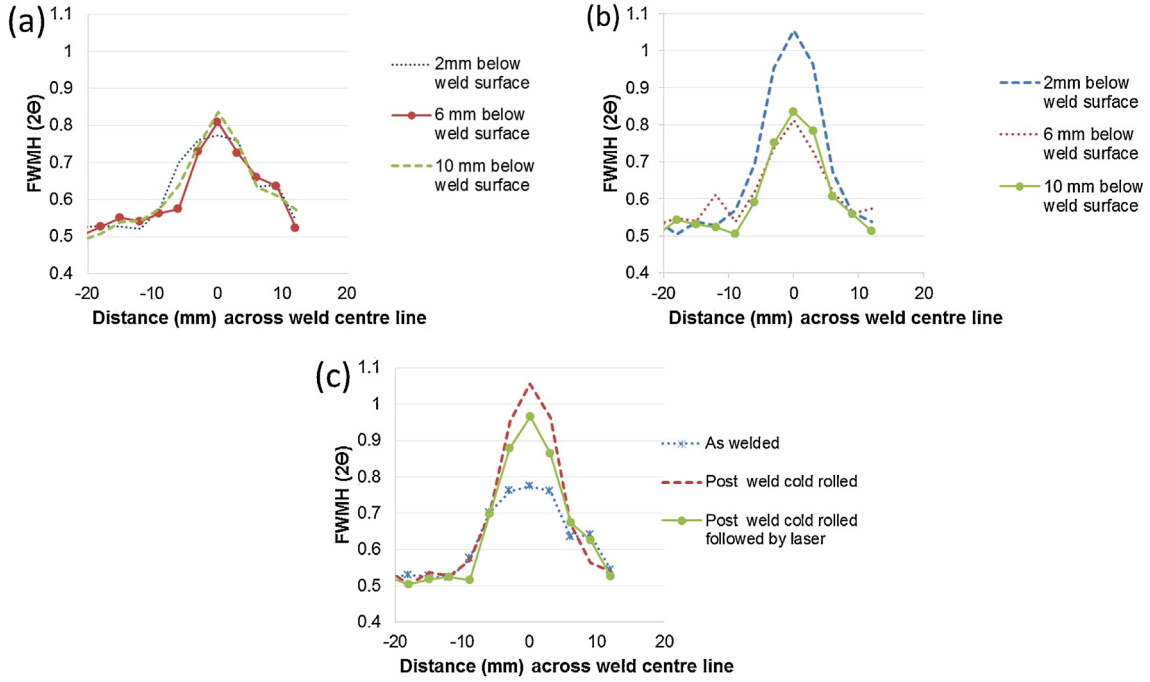

Fig. 13. Effect of FWHM on plastic deformation at (a) As-welded at 2, 6, and 10 mm below weld surface (b) Post weld cold rolled at 2, 6 and 10 mm below weld surface (c) The three samples at 2 mm below weld surface.

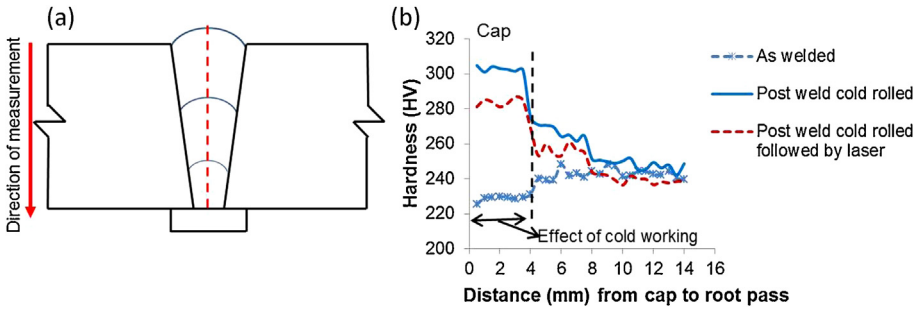

Fig. 14. Showing (a) hardness scan position along the weld metal and (b) hardness profile.

However, post weld cold rolled followed by laser processing softened the weld metal due to annealing of the strain hardened which caused a fall in proof stress. This softening of the grain structure indicates refining the grains which will therefore improve the mechanical properties of the weld metal.

As show in Fig. 16, during welding and subsequent cooling of material, residual stresses are generated in weldments due to differential heating and cooling rates [1,30]. When this material is cooling after welding, the stresses generated may exceed the yield strength, causing plastic deformation and work hardening in the weld metal. Since the root regions experience more thermal cycles than any other region, they undergo more thermal straining. The enhanced plastic deformation in the root regions is responsible for the high hardness values observed in the root pass. The increase in hardness at the root pass (as-welded) could also be attributed to increase in chromium content in weld metal (which is about

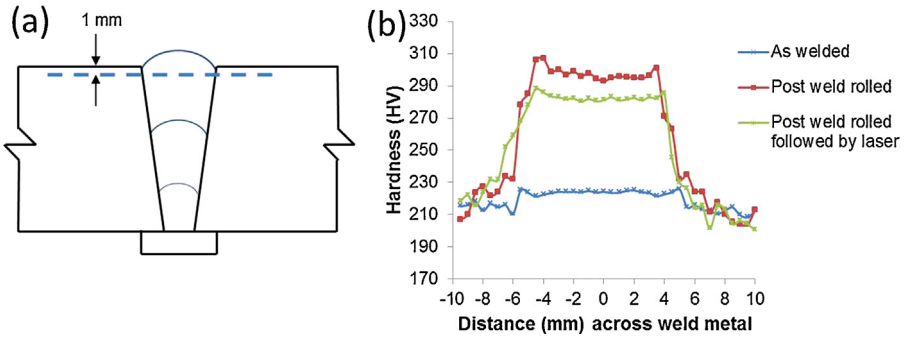

Fig. 15. Showing (a) hardness scan position (b) Hardness profile across the cap pass of three samples.

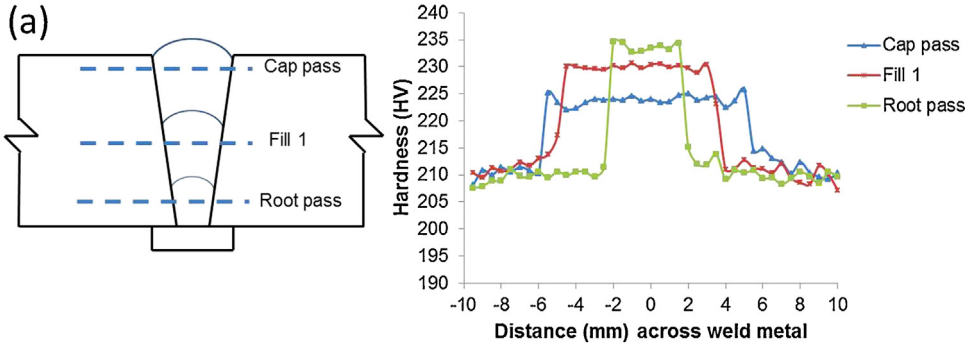

Fig. 16. As- welded (a) hardness scan position (b) Hardness profile across the multi-pass welds.

20.43 wt%), since high chromium content combining with niobium presence in the weld metal increases steel hardenability. The scattering of the hardness values could be due to placement of indentation within the weld metal since each pass has a different microstructure as a result of the re-heating by subsequent passes.

3.6. Tensile strength

Fig. 17 shows the ultimate tensile strength (UTS), the 0.2% proof strength (PS) and the percentage elongation (%EL). Post weld cold rolling increases the ultimate tensile strength and proof strength, and decrease the ductility. While, post weld cold rolled followed by laser processing decreases the ultimate tensile strength and proof strength, and show a slight increase in the ductility.

As shown in Fig. 17, post weld cold rolled brought about 31% increase in ultimate tensile strength (526 MPa–690 MPa) and 36% increase in proof strength (393 MPa–534 MPa) with corresponding reduction in percentage elongation (50.5–37.5%) in the fusion zone. Of course one of the main mechanism by which plastic deformation takes place is the slip of dislocations. The post weld cold rolling increases dislocation density which restricts the slipping of dislocations. In other word, plasticity of the material reduces due to cold working. This results in lowering of ductility and increase the strength. Post weld cold rolled lead to increase in proof strength as well as increase in hardness (Fig. 15) in the fusion zone (cap pass) indicating that proof stress and Vickers hardness are roughly related.

Post weld cold rolling followed by laser processing brought about 9% decrease in UTS and 7% decrease in PS and slight increase in percentage elongation (37.5–39.5%). This indicates that, some of the stored internal strain energy was relieved as a result of enhanced atomic diffusion at higher temperature. An effective indication of recrystallization can be drop in proof strength [31] due to releasing of internal energy; the greater the amount of prior deformation, the lower the temperature to initiate recrystallization, as the activation energy gap needed to initiate recrystallization would be less.

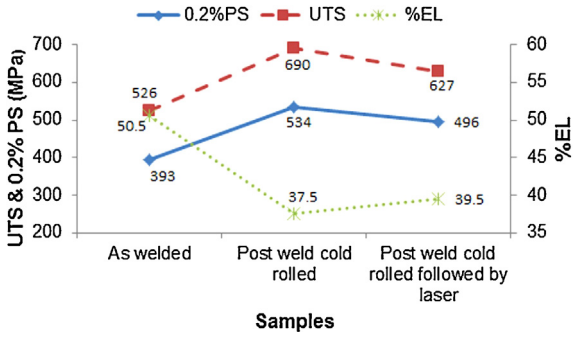

Fig. 17. Tensile test showing the effect of both post weld cold rolled and post weld cold rolled followed by laser processing.

4. Conclusions

This paper investigates the possibilities of using local mechanical tensioning (rolling) followed by laser treatment to create a refined and recrystallized microstructure with modified residual stress state, thus improving the fatigue life of welded structures. It can therefore be deduced from the experiments that:

Very minimal grains refinement was observed at the cap pass of multi-pass welds when post weld cold rolling followed by laser processing was applied to the sample. This refine grain (average grain size of 11.00 μm) in laser processed samples would, therefore, have the potential of improving the strength and toughness of the weld metal.

The post weld cold rolling modifies the tensile residual stress state, and a compressive residual stress was formed below the weld metal. As the modification of stress state is achieved by plastic deformation, 31% increase in ultimate tensile strength and 36% increases in proof strength with corresponding reduction in percentage elongation (50.5–37.5%) in the fusion zone was observed.

Although, post weld cold rolling followed by laser processing resulted in formation of minimal refined microstructure. The recrystallisation is not sufficient because of the transient thermal cycle is not sufficient to supply enough energy to sustain the recrystallization kinetics. However, laser processing reinstated as-welded residual stress state profile with even higher magnitude of peak stress.

Peak tensile residual stress of the as-welded sample diminishes in magnitude through the thickness of a multi-pass welds. This is attributed to the fact that, multiple passes result in thermal straining of previously laid pass from successive passes. The thermal cycling would cause macroscopic plastic deformation of previously laid passes.

FWHM in this experiment shows an increase with increase in plastic deformation (post weld cold rolled). FWHM in terms of residual stress state shows that, increase in FWHM modify the tensile residual stress to compressive stress state. Post weld cold rolling followed by laser processing reduces the peak of FWHM.

Acknowledgements

The authors are grateful for the funding provided by Petroleum Development Trust Fund in Nigeria, under the PTDF scholarship scheme no. PTDF/E/OSS/PHD/SJ/391/11. The authors are also thankful to Dr. Xianwei Liu for his support during SEM analysis. Dr Supriyo Ganguly acknowledges support from EPSRC through grant numbers EP/J017086/1 and EP/K030884/1.

References

[1] Cary HB. Modern welding technology. 2nd ed USA: Amercian Welding Society; 1981. p. 497–8.
[2] Liao MT, Chen WJ. The influence of shielding gas on notch toughness of stainless steel weld metals. Mater Manuf Process 1998;13(4):565–73.
[3] Karci F, Kaçar R, Gündüz S. The effect of process parameter on the properties of spot welded cold deformed AISI304 grade austenitic stainless steel. J Mater Process Technol 2009;209(8):4011–9.
[4] Baek J-, Kim Y-, Kim W-, Kho Y-. Fracture toughness and fatigue crack growth properties of the base metal and weld metal of a type 304 stainless steel pipeline for LNG transmission. Int J Press Vessel Pip 2001;78(5):351–7.
[5] Smith WF. Structure and properties of engineering alloys. 2nd ed New York: McGraw-Hill; 1993.
[6] Cho JR, Lee BY, Moon YH, Van Tyne CJ. Investigation of residual stress and post weld heat treatment of multi-pass welds by finite element method and experiments. J Mater Process Technol 2004;155–156(1–3):1690–5.
[7] Lippold JC, Kotecki DJ. In: Lippold JC, Kotecki DJ, editors. Welding metallurgy and weldability of stainless steels. Hoboken, NJ: John Wiley & Sons Inc.; 2005.
[8] Kou S. Welding metellury. 2nd ed Hoboken, New Jersey., Canada: John Wiley & Sons, Inc.; 2003.
[9] Panchal VD. Relieving stress in stainless steels. World Pumps 2013;2013(1):28–32.
[10] Moat RJ, Stone HJ, Shirzadi AA, Francis JA, Kundu S, Mark AF, et al. Design of weld fillers for mitigation of residual stresses in ferritic and austenitic steel welds. Sc Technol Weld Join 2011;16(3):279–84.
[11] Jurcius, A. and Valiulis, A.V. (2008), Reduce of material residual stresses using vibration energy, *Vibrofngineering 2008—Proceedings of 7th International Conference*, pp. 50.
[12] Rao D, Chen L, Ni C. Vibratory stress relief of welded structure in China. Mater High Temp 2006;23(3–4):245–50.
[13] Yanagida N, Koide H. Residual stress improvement in multi-layer welded plates using water-shower cooling during welding process. Nihon Kikai Gakkai Ronbunshu, A Hen/Trans Jpn Soc Mech Eng, Part A 2006;72(11):1631–8.
[14] Nadzam J. Tandem GMAW: the flexibilty of pulsed spray transfer. Weld Innov 2002;19(2):12–5.
[15] Hudson MG. Welding of X100 linepipe. Cranfield, UK: Cranfield University; 2004 (PhD thesis).
[16] Theocharis L. Tandem gas metal arc pipeline welding. Cranfield, UK: Cranfield University; 2007 (PhD thesis).
[17] Pirling T, Bruno G, Withers PJ. SALSA-A new instrument for strain imaging in engineering materials and components. Mater Sci Eng A 2006;437(1):139–44.
[18] Withers PJ, Turski M, Edwards L, Bouchard PJ, Buttle DJ. Recent advances in residual stress measurement. Int J Press Vessel Pip 2008;85(3):118–27.
[19] Rogante M. Stress-free reference sample: the problem of the determination of the interplanar distance d0. Phys B: Condens Matter 2000;276–278:202–3.
[20] Holden TM, Suzuki H, Carr DG. Macroscopic stress measurements by neutron diffraction and the part played by the "stress-free" reference. ISIJ Int 2006;46(7):959–65.
[21] Withers PJ, Bhadeshia HKDH. Residual stress part 1—measurement techniques. Mater Sci Technol 2001;17(4):355–65.
[22] ASM Aerospace Specification Metals, Inc. (2015), *AISI Type 304 Stainless Steel—ASM Material Data Sheet*, Available at: ⟨http://asm.matweb.com/search/SpecificMaterial.asp?bassnum=MQ304A⟩.[accessed 01.06].
[23] Moore, M.G. and Evans, W.P. (1958), Mathematical correction for stress in removed layers in X-ray diffraction residual stress analysis, *SAE Technical Papers*.
[24] Tung H-, Huang J-, Tsai D-, Ai C-, Yu G-. Hardness and residual stress in nanocrystalline ZrN films: effect of bias voltage and heat treatment. Mater Sci Eng A 2009;500(1–2):104–8.
[25] Vivek,R., Binayaka, N., Mohd, Z., Meghanshu, V. (2013), *Assessment of Plastic Deformation Upon Grainding Using X-Ray Diffraction Profiles*, Available at: ⟨http://www.ijer.in/ijer/publication/v2s2/paper20.pdf⟩.[accessed 08.06].
[26] Quesnel, D.J., Meshii, M. and Cohen, J.B., (1978), Residual stresses in high strength low alloy steel during low cycle fatigue.
[27] Mitra A, Srivastava PK, De PK, Bhattacharya DK, Jiles DC. Ferromagnetic properties of deformation-induced martensite transformation in AISI 304 stainless steel. Metall Mater Trans A: Phys Metall Mater Sci 2004;35 A(2):599–605.
[28] Peguet L, Malki B, Baroux B. Influence of cold working on the pitting corrosion resistance of stainless steels. Corros Sci 2007;49(4):1933–48.
[29] Garda C. Effect of prior cold work on intergranular and transgranular corrosion in type 304 stainless steels: quantitative discrimination by image analysis. Corrosion 2000;56(3):243–55.
[30] Masubuchi K. Analysis of welded structures. Oxford: Pergamon Press; 1980.
[31] Avner SH. Introduction to physical metallurgy. 2nd ed Tokyo: McGraw Hill Kogakusha; 1974.

Application of local mechanical tensioning and laser processing to refine microstructure and modify residual stress state of a multi-pass 304L austenitic steels welds

Sule, Jibrin

2015-03-03

Sule J, Ganguly S, Coules H, Pirling T. (2015) Application of local mechanical tensioning and laser processing to refine microstructure and modify residual stress state of a multi-pass 304L austenitic steels welds. Journal of Manufacturing Processes, Volume 18, April 2015, pp. 141-150
http://dx.doi.org/10.1016/j.jmapro.2015.03.003